Tricellular junctions regulate intestinal stem cell behavior to maintain homeostasis

Martin Resnik-Docampo[1], Christopher L. Koehler[1], Rebecca I. Clark[2,*], Joseph M. Schinaman[2], Vivien Sauer[1], Daniel M. Wong[1], Sophia Lewis[1], Cecilia D'Alterio[1], David W. Walker[2,3] and D. Leanne Jones[1,3,4,#]

[1] Department of Molecular, Cell, and Developmental Biology, [2]Department of Integrative Biology and Physiology, [3]Molecular Biology Institute, [4]Eli and Edythe Broad Center of Regenerative Medicine and Stem Cell Research, University of California, Los Angeles, Los Angeles, CA 90095, USA.

[#]To whom correspondence should be addressed: Leanne Jones

Postal address: University of California, Los Angeles
Department of Molecular, Cell, and Developmental Biology
5139 Terasaki Life Sciences Building
Los Angeles, CA 90095

Telephone number: (310) 206-7066
Email Address: leannejones@ucla.edu

[*] Present Address: School of Biological and Biomedical Sciences, Durham University, Durham DH1 3LE, UK

Running title: Tricellular junctions regulate intestinal stem cell behavior

Key words: stem cell, intestine, *Drosophila*, Gliotactin, occluding junctions, tricellular junctions, aging

Aging results in loss of tissue homeostasis across taxa[1]. In the intestine of *Drosophila melanogaster*, aging is correlated with an increase in intestinal stem cell (ISC) proliferation, a block in terminal differentiation of progenitor cells, activation of inflammatory pathways, and increased intestinal permeability [2]. However, causal relationships between these phenotypes remain unclear. Here, we demonstrate that aging results in altered localization and expression of Septate Junction (SJ) proteins in the posterior midgut, which is quite pronounced in differentiated enterocytes (ECs) at tricellular junctions (TCJ). Acute loss of the TCJ protein Gliotactin (Gli) in ECs results in increased ISC proliferation and a block in differentiation in intestines from young flies, demonstrating that compromised TCJ function is sufficient to alter ISC behavior in a non-autonomous manner. Blocking the Jun N-terminal kinase (JNK) signaling pathway is sufficient to suppress changes in ISC behavior, but has no effect on loss of intestinal barrier function, as a consequence of Gli depletion. Our work demonstrates a pivotal link between TCJ, stem cell behavior, and intestinal homeostasis and provides new insights into causes of age-onset and gastrointestinal diseases.

The intestinal epithelium provides a selective barrier that permits nutrient and water transport, while preventing uptake of harmful environmental toxins and microbial contamination of interstitial tissues[3]. In addition to its barrier function, the intestinal epithelium serves essential roles in metabolism and immunity. Highly specialized intercellular occluding junctions, referred to as tight junctions (TJ) in chordates and septate junctions (SJ) in arthropods, maintain this critical barrier. The *Drosophila* midgut epithelium is composed of intestinal stem cells (ISCs) that self-renew to maintain the ISC pool and produce daughter cells, known as enteroblasts (EBs), which can differentiate into either secretory enteroendocrine (EE) cells or absorptive enterocytes (ECs) (Supplementary Fig. 1A)[4, 5]. In the *Drosophila* midgut, SJ exist between adjacent ECs and between ECs and EE cells, both of which are located apically and are in contact with the intestinal lumen (Fig. 1A, Supplementary Fig. 1A). Therefore, we hypothesized that age-related changes in SJ could directly contribute to loss of intestinal barrier function. Furthermore, given the significant role that differentiated cells play in regulating ISC behavior in the intestine[6, 7], we speculated that changes in SJ could contribute in a non-autonomous manner to altered ISC behavior over time.

Consistent with the loss of barrier function in older animals[8, 9], electron microscopy revealed distinct gaps in SJ between adjacent ECs in midguts from old wild type (WT) flies, which were not observed in midguts from young flies (Fig. 1A-B). In order to determine whether the compromised SJ function in aged intestines could be due to decreased gene expression, RNAseq analysis was performed on posterior midguts from young (5do) and old (45do) flies. These data revealed that 38% (18/48) of genes annotated as being involved in SJ or SJ assembly (Gene Ontology terms GO:0005918 and GO:00019991) exhibited changes in expression (Fig. 1C; Supplementary Table1), and an enriched analysis of the dataset revealed that the "cell adhesion" gene ontology (GO) category was one of the most representative GO categories that change with age (Supplementary Table1). The expression level of the majority of these genes (16 of 18) was up-regulated in old flies, indicating that decreased transcription is not a primary mechanism contributing to age-related changes in SJs in the midgut.

In *Drosophila*, SJ are divided into two classes based on morphological appearance: pleated SJ (pSJ) are found in ectodermally-derived tissues, such as the hindgut, while smooth SJ (sSJ) are observed in endodermally-derived tissues, including the midgut [10]. To evaluate possible age-related changes in SJ protein localization or expression, confocal and super-resolution immunofluorescence microscopy were used to visualize smooth and pleated SJ proteins in midguts and hindguts, respectively (Fig. 1 D-M, Supplementary Fig. 1 B-O,R-S). In 45do flies, significant changes in SJ proteins Discs large (Dlg), Coracle (Cora), Scribble (Scrib), Snakeskin (Ssk) and Mesh were observed in the midgut: Dlg, Cora, and Scrib showed decreased staining intensity, due to an apparent separation of adjacent cell membranes, while Ssk and Mesh appeared to accumulate in the cytoplasm (Fig. 1D-M). These changes were quantified by measuring the ratio of staining intensities at the membrane (SJ/cytoplasm) (Fig. 1 P-T). In contrast, Dlg, Cora, and Scrib levels were not decreased in the hindgut (Supplementary Fig. 1J-O). Furthermore, levels of Armadillo (Arm), an Adherens Junctions (AJ) component, did not appear affected by age in midguts or hindguts (Fig. 1N-O,V; Supplementary Fig. 1R-S).

One striking and consistent age-related change in SJs was observed at tricellular junctions (TCJ) (arrowheads, Fig. 1D-I, L-M, P-T), the specialized junction at the conjunction of three cells[11]. Gliotactin (Gli) is one of two SJ proteins that have been described in *Drosophila* to localize to the TCJ[12-14], and Gli has been demonstrated to

play a role in the developing nervous system[15] and imaginal discs[12, 16]. However, a role in the adult intestine has not yet been evaluated.

In the adult posterior midgut, Gli co-localized with Dlg (Fig. 2A-B'; Supplementary Fig. 2A-A''), as described previously in wing discs[16, 17]. Gli protein was clearly detected at EC-EC and EC-EE cell TCJ (Fig. 2 A,C,F); however, no Gli protein was detected in ISCs/EBs (Fig. 2D). In midguts from aged flies, Gli localization was largely absent from the TCJ, and protein levels were increased in the cytoplasm (Fig. 2F-H). In hindguts, no changes in Gli localization or protein levels were observed, similar to our observation for other SJ proteins (Supplementary Fig. 1P-Q). Interestingly, Dlg appeared cytoplasmic, rather than membrane-localized, in ISC/EB 'nests', suggesting that definitive SJ may be absent between ISC/EBs and that formation of SJ is coordinated with differentiation. Consistent with this hypothesis, SJ were not apparent between ISCs and EBs via EM (Fig. 2E).

Given the significant changes in TCJ (Fig. 1 D-M, P-T) and the striking loss of Gli from TCJ in older animals (Fig. 2G-H), we tested whether these changes were, indeed, a consequence of aging. Dietary restriction (DR) is the most robust and reproducible intervention known to slow aging across species [18]. Changes in Gli localization were delayed in long-lived, DR flies, when compared to controls, indicating that physiological age was a significant factor contributing to changes in TCJ (Fig. 2I, J)

To determine whether compromised TCJ function could contribute to age-related changes in the intestine, Gli was depleted from TCJs using a drug-inducible version of the GAL4-UAS system[19, 20]. Targeted gene expression using the *5966^{GS}* GAL4 "driver" is observed in adult ECs when flies are fed the progesterone analog RU486; addition of EtOH is used as a control, providing cohorts of isogenic individuals with or without induction of a *Gli^{RNAi}* transgene. Efficacy of *Gli^{RNAi}* was confirmed by immunostaining and RT-qPCR (Supplementary Fig. 2B-D).

Depletion of Gli from ECs resulted in an accelerated loss of barrier integrity (Fig. 3A ; Supplementary Fig. 2E). Integrity of the intestinal barrier can be assayed by feeding flies a non-absorbable blue food dye. When the intestinal barrier is intact, the dye is retained within the intestine, whereas loss of barrier integrity results in spreading of blue dye throughout the hemolymph (generating "Smurf" flies) [8, 9]. Reduced *Gli* expression in ECs led to a significant increase in "Smurf" flies as early as 12 days after *Gli^{RNAi}* expression, when compared to age-matched controls (Fig. 3A; Supplementary Fig. 2E). EM analysis of midguts from 23do flies revealed no noticeable changes in SJ structure

at bicellular junctions when Gli was depleted from ECs (Supplementary Fig.2F-G), indicating that loss of barrier function was due to disruption of TCJ, rather than disruption of the entire SJ. At 40 days, 94.7% of the *Gli*^{RNAi} population exhibited the "Smurf" phenotype, compared to 57.1% of controls (Fig. 3A), with a concomitant decrease in median lifespan (Supplementary Fig. 2H).

Upon Gli depletion from ECs for 23 days, the localization of SJ proteins was altered similar to what was observed in intestines from aged flies (compare Figs. 1D-M to Figs. 3 C,E,G,I). Neither protein levels nor localization was affected in controls (Fig. 3B, D,F,H). In epithelia of imaginal discs, Dlg is needed to recruit Gli into TCJ, but not *vice versa* [16]. This relationship is maintained in the midgut, as depletion of Gli had only a modest affect on TCJ Dlg enrichment (arrowheads, Fig. 3B,C), whereas depletion of Dlg from ECs led to a complete loss of Gli from TCJ (Fig. 3J-M). Altogether, these data indicate that depletion of Gli from the TCJ, rather than mis-localization of Dlg and complete disruption of SJ, is sufficient to trigger loss of barrier integrity.

In the *Drosophila* midgut, aging, stress, or increased inflammation results in a dramatic increase in ISC proliferation, which is accompanied by an accumulation of mis-differentiated daughter cells that express hallmarks of both ISCs and terminally differentiated enterocytes [6, 21, 22]. A statistically significant increase in number of cells expressing the ISC/EB marker Esg was observed upon *Gli* depletion from ECs for 9 days (Fig. 4C-D,E). In addition, an increase in ISC proliferation was observed, based on the mitosis marker phosphorylated histone H3 (PH3) (Fig. 4D,F). Similar results were obtained using two additional *Gli*^{RNAi} lines (Supplementary Fig. 3A-D). After 9 days of *Gli* depletion, flies were shifted onto RU- food to re-initiate Gli expression for 11 days. Re-expression of Gli in ECs resulted in resumption of normal ISC behavior (Supplementary Fig. 3G-K), indicating that changes in ISCs are directly correlated with the presence of Gli and that loss of TCJ integrity is reversible under these conditions. Depletion of Gli specifically from EEs did not result in any changes in ISC behavior (Supplementary Fig. 3L). Reduced expression of Dlg in ECs resulted in similar effects on ISC behavior (Supplementary Fig. 3E-F). However, as noted above, depletion of Dlg resulted in a complete loss of Gli from TCJ; therefore, the effects of Dlg depletion cannot be uncoupled from an effect on Gli. These data indicate that depletion of Gli from differentiated ECs is sufficient to induce age-related phenotypes, including loss of barrier function and changes in ISC behavior, in intestines of young flies.

Finally, to address whether increased ISC proliferation, in response to Gli depletion, was due to death of ECs via apoptosis, anti-apoptotic factors dIAP and P35 were individually co-expressed with *Gli*^{RNAi} in ECs. Co-expression of dIAP or P35 with *Gli*^{RNAi} was not sufficient to suppress the increase of *esg*+ cells or ISC proliferation; no effect on ISC behavior was observed in controls (Supplementary Fig. 4A-F). Therefore, our data indicate that apoptosis does not play a critical role downstream of Gli to trigger non-autonomous changes in ISC behavior.

Increased microbial loads and a disruption in the composition of commensal bacteria in aged flies, collectively referred to as dysbiosis, has been shown to contribute to cellular changes in the aging intestine, including an increase in ISC proliferation [23-26]. To test whether the presence of bacteria could impact ISC behavior, upon Gli depletion, we generated *5966*^{GS}*GAL4/UAS-Gli*^{RNAi} flies under axenic conditions and examined ISC behavior in young flies (Supplementary Fig. 4I). Axenic flies in which Gli was depleted exclusively from ECs showed a similar increase in the number of cells expressing the ISC/EB marker Esg, as well as an increase in ISC mitoses, when compared to flies reared under conventional, non-sterile conditions (Fig. 4G-J). Altogether, our data suggest that changes in bacterial populations are not a major contributing factor to accelerated ISC proliferation and intestinal dysplasia observed upon depletion of Gli.

To determine possible mechanisms by which Gli depletion could elicit alterations in stem cell behavior, changes in gene expression were assessed in posterior midguts from control flies or flies depleted of Gli for 2 or 9 days. At the 9-day time point, *Gli* expression was decreased and *esg* expression increased, presumably due to the increase in the *esg*+ cells, compared to controls (Supplementary Table 2). Comprehensive analysis of the RNAseq dataset revealed an increase in activity of pathways known to stimulate ISC proliferation in response to damage, infection, or stress, including the Jun-N-terminal Kinase (JNK), Hippo, Epidermal Growth Factor (EGF), Wingless (Wg) and Janus kinase-Signal Transducer and Activator of Transcription (JAK/STAT) pathways [2] (Supplementary Table 2). Upregulation of genes encoding SJ proteins, such as *dlg, mesh, cora* and *Ssk,* was observed, similar to the age-related changes in expression detected in midguts from aged flies (Fig. 1C; Supplementary Tables 1, 2). However, an increase in expression of AMPs was not detected, suggesting that the increase in ISC proliferation is not due to an inflammatory

response as a result of bacterial dysbiosis[23,26] (Supplementary Fig. 3M-N and Supplementary Table 2).

The JNK pathway is a highly conserved stress-sensing pathway that regulates gene expression, regeneration, apoptosis and metabolic adaptation in response to both extrinsic and intrinsic stressors [27]. In the intestine, activation of the JNK pathway in ECs leads to increased expression of cytokine-like molecules that, in turn, activate the JAK-STAT pathway in ISCs to stimulate ISC proliferation [2, 6, 7, 28]. Therefore, we wanted to determine whether JNK pathway activation could be responsible for driving the ISC response downstream of *Gli* depletion.

Activation of the JNK pathway was observed in ECs as early as 2 days after *Gli* depletion, in comparison to controls, as determined by expression of a downstream target of the pathway, *puckered* (*puc*) (Fig. 5A-F'). Similar results were observed when the experiment was conducted under axenic conditions (Supplementary Fig. 4G-H'). An increase in *puc* expression upon *Gli* depletion was confirmed by RT-qPCR and RNAseq analysis (Supplementary Fig. 4J and Table 2). Suppression of JNK signaling in ECs, achieved by ectopic expression of a dominant negative version of the single *Drosophila* JNK, *basket* (bsk^{DN}), had no effect on ISC behavior in controls (Fig. 5 G-H,K-L,O-P). However, expression of bsk^{DN} was sufficient to suppress the increase in *esg*-expressing cells and ISC proliferation in response to EC-specific *Gli* depletion (Fig. 5I-J,M-P). In contrast, co-expression of bsk^{DN} was not sufficient to suppress the loss of barrier integrity, nor the decrease in survival, observed upon Gli^{RNAi} (Fig. 5Q; Supplementary Fig. 4K), suggesting that activation of JNK at early time points does not contribute to loss of barrier function. Altogether, these data indicate that JNK signaling is activated downstream of TCJ to drive changes in ISC behavior in a non-autonomous manner.

Our data indicate that aging results in changes to occluding junctions that likely contribute to the loss of barrier integrity described previously[8, 9]. However, acute depletion of the TCJ protein Gli in young flies quickly led to hallmarks of aging, including an increase in ISC proliferation and a block in terminal differentiation. Surprisingly, changes in ISC behavior were observed prior to loss of the permeability barrier, activation of AMPs, and increases in bacterial populations (Figs. 3,4). While not all phenotypes associated with aging are observed upon dowregulation of Gli at early time points, our data suggest that altered TCJ function during the course of normal aging could contribute directly to the changes in ISC behavior observed in older animals.

Although age-dependent remodeling of epithelial junctions has been described in mammalian models [29-31], no prior link between changes in occluding junctions and age-related changes in stem cell behavior has been established in other systems. If this connection is conserved in mammalian systems, epithelial remodeling could be a driver of a host of intestinal diseases, including colon cancer. Furthermore, if age-related changes to occluding junctions also occur within tissues in which low or no turnover takes place, loss of barrier function could be a substantial contributing factor to age-onset or degenerative diseases in tissues such as the nervous system, ear, or the kidney.

Acknowledgements

The authors thank H. Jasper, V. Auld, J.F. de Celis, M. Furuse, the Vienna Drosophila RNAi Center (VDRC), and Bloomington Stock Center for reagents, Marianne Cilluffo from the Brain Research Institute at UCLA EM core facility, and the Jones and Walker laboratories for comments on the manuscript. In addition, we would like to thank Drs. Yong Wu and Enrico Stefani for their sharing their time, expertise, and STED technology. This work was supported by the Eli and Edythe Broad Center of Regenerative Medicine and Stem Cell Research at the University of California- Los Angeles and the Rose Hills Foundation (D.L.J), and the NIH: AG028092 (D.L.J.), AG040288 (D.L.J. and D.W.W.), AG049157 (D.W.W.), and a training grant which supports the UCLA-Caltech Medical Scientist Training Program, GM08042 (S.L.).

Author Contributions

M.R.D. designed, performed, and analyzed experiments and wrote the manuscript. C.L.K., R.I.C, J.M.S, D.M.W., V.S., S.L., and C.D. designed, performed and analyzed experiments. D.W.W. designed and analyzed experiments. D.L.J. designed and analyzed experiments and wrote the manuscript.

References

1. Jones, D.L. & Rando, T.A. Emerging models and paradigms for stem cell ageing. *Nature cell biology* **13**, 506-512 (2011).
2. Li, H. & Jasper, H. Gastrointestinal stem cells in health and disease: from flies to humans. *Disease models & mechanisms* **9**, 487-499 (2016).
3. Marchiando, A.M., Graham, W.V. & Turner, J.R. Epithelial barriers in homeostasis and disease. *Annual review of pathology* **5**, 119-144 (2010).
4. Micchelli, C.A. & Perrimon, N. Evidence that stem cells reside in the adult Drosophila midgut epithelium. *Nature* **439**, 475-479 (2006).
5. Ohlstein, B. & Spradling, A. The adult Drosophila posterior midgut is maintained by pluripotent stem cells. *Nature* **439**, 470-474 (2006).
6. Biteau, B., Hochmuth, C.E. & Jasper, H. JNK activity in somatic stem cells causes loss of tissue homeostasis in the aging Drosophila gut. *Cell stem cell* **3**, 442-455 (2008).
7. Jiang, H. *et al.* Cytokine/Jak/Stat signaling mediates regeneration and homeostasis in the Drosophila midgut. *Cell* **137**, 1343-1355 (2009).
8. Rera, M. *et al.* Modulation of longevity and tissue homeostasis by the Drosophila PGC-1 homolog. *Cell metabolism* **14**, 623-634 (2011).
9. Rera, M., Clark, R.I. & Walker, D.W. Intestinal barrier dysfunction links metabolic and inflammatory markers of aging to death in Drosophila. *Proceedings of the National Academy of Sciences of the United States of America* **109**, 21528-21533 (2012).
10. Tepass, U. & Hartenstein, V. The development of cellular junctions in the Drosophila embryo. *Developmental biology* **161**, 563-596 (1994).
11. Fristrom, D.K. Septate junctions in imaginal disks of Drosophila: a model for the redistribution of septa during cell rearrangement. *The Journal of cell biology* **94**, 77-87 (1982).
12. Schulte, J., Tepass, U. & Auld, V.J. Gliotactin, a novel marker of tricellular junctions, is necessary for septate junction development in Drosophila. *The Journal of cell biology* **161**, 991-1000 (2003).
13. Byri, S. *et al.* The Triple-Repeat Protein Anakonda Controls Epithelial Tricellular Junction Formation in Drosophila. *Developmental cell* **33**, 535-548 (2015).
14. Hildebrandt, A. *et al.* Bark beetle controls epithelial morphogenesis by septate junction maturation in Drosophila. *Developmental biology* **400**, 237-247 (2015).
15. Auld, V.J., Fetter, R.D., Broadie, K. & Goodman, C.S. Gliotactin, a novel transmembrane protein on peripheral glia, is required to form the blood-nerve barrier in Drosophila. *Cell* **81**, 757-767 (1995).
16. Schulte, J. *et al.* Gliotactin and Discs large form a protein complex at the tricellular junction of polarized epithelial cells in Drosophila. *Journal of cell science* **119**, 4391-4401 (2006).
17. Padash-Barmchi, M., Charish, K., Que, J. & Auld, V.J. Gliotactin and Discs large are co-regulated to maintain epithelial integrity. *Journal of cell science* **126**, 1134-1143 (2013).
18. Fontana, L., Partridge, L. & Longo, V.D. Extending healthy life span--from yeast to humans. *Science* **328**, 321-326 (2010).
19. Osterwalder, T., Yoon, K.S., White, B.H. & Keshishian, H. A conditional tissue-specific transgene expression system using inducible GAL4. *Proceedings of the National Academy of Sciences of the United States of America* **98**, 12596-12601 (2001).

20. Roman, G., Endo, K., Zong, L. & Davis, R.L. P[Switch], a system for spatial and temporal control of gene expression in Drosophila melanogaster. *Proceedings of the National Academy of Sciences of the United States of America* **98**, 12602-12607 (2001).
21. Choi, Y.J. *et al.* Age-related upregulation of Drosophila caudal gene via NF-kappaB in the adult posterior midgut. *Biochimica et biophysica acta* **1780**, 1093-1100 (2008).
22. Park, J.S., Kim, Y.S. & Yoo, M.A. The role of p38b MAPK in age-related modulation of intestinal stem cell proliferation and differentiation in Drosophila. *Aging* **1**, 637-651 (2009).
23. Buchon, N., Broderick, N.A., Chakrabarti, S. & Lemaitre, B. Invasive and indigenous microbiota impact intestinal stem cell activity through multiple pathways in Drosophila. *Genes & development* **23**, 2333-2344 (2009).
24. Buchon, N., Broderick, N.A. & Lemaitre, B. Gut homeostasis in a microbial world: insights from Drosophila melanogaster. *Nature reviews. Microbiology* **11**, 615-626 (2013).
25. Guo, L., Karpac, J., Tran, S.L. & Jasper, H. PGRP-SC2 promotes gut immune homeostasis to limit commensal dysbiosis and extend lifespan. *Cell* **156**, 109-122 (2014).
26. Clark, R.I. *et al.* Distinct Shifts in Microbiota Composition during Drosophila Aging Impair Intestinal Function and Drive Mortality. *Cell reports* **12**, 1656-1667 (2015).
27. Biteau, B., Karpac, J., Hwangbo, D. & Jasper, H. Regulation of Drosophila lifespan by JNK signaling. *Experimental gerontology* **46**, 349-354 (2011).
28. Staley, B.K. & Irvine, K.D. Warts and Yorkie mediate intestinal regeneration by influencing stem cell proliferation. *Current biology : CB* **20**, 1580-1587 (2010).
29. Meier, J. & Sturm, A. The intestinal epithelial barrier: does it become impaired with age? *Digestive diseases* **27**, 240-245 (2009).
30. Ren, W.Y. *et al.* Age-related changes in small intestinal mucosa epithelium architecture and epithelial tight junction in rat models. *Aging clinical and experimental research* **26**, 183-191 (2014).
31. Tran, L. & Greenwood-Van Meerveld, B. Age-associated remodeling of the intestinal epithelial barrier. *The journals of gerontology. Series A, Biological sciences and medical sciences* **68**, 1045-1056 (2013).

Figure Legends:

FIG. 1: Age-related changes in septate junctions (SJ) in posterior midguts from aged flies. (A-B) EM images showing a gap at the SJ (arrowhead) between ECs in an intestine from a 45 days old (do) fly (B) compared to SJ between adjacent ECs in a gut from a 5do fly (young) (A); n=6 midguts per condition (n=10 EC/EC SJs were observed per midgut). Scale bars 0.1µm. (C) Expression heatmap of representative changes in gene expression (old/young) of genes encoding SJ or SJ assembly components that change with age. (D-O) STED images comparing SJ protein localization in ECs in young (10do) or aged (45 do) midguts. SJ protein mis-localization is observed in old ECs, represented by thicker bicellular junctions, disappearance of enriched SJ protein localization at TCJ (arrowheads, D, F, H, L compared to E, G, I, M respectively) and an increase in cytoplasmic localization (K, M). (N-O) STED images showed the AJ protein Arm is not affected by aging. n=>14 midguts per condition; n=10 ECs were observed per midgut. Samples were dissected and stained in parallel under same conditions, pictures taken at same laser intensity. (P-V) TCJ/Cytoplasm (red) and bicellular SJ/Cytoplasm (grey) fluorescence ratios for different SJ and AJ components. Data analyzed with ONE-way ANOVA/Tukey's multiple comparisons test and the error bars are the SEM range of those averages. **** = P<0.0001 , *** = P<0.001, ** = P< 0.01, * = P<0.05 represent a statistically significant difference. (P) Discs large (5do n=20; 45do n=19). (Q) Coracle (5do n=27; 45do n=22). (R) Scribble (5do n=20; 45do n=21). (S) Snakeskin (5do n=21; 45do n=20). (T) Mesh (5do n=21; 45do n=21). (V) Armadillo (5do n=20; 45do n=21). Each data point (n= midguts) represents an average fluorescence intensity ratio from 2-7 independent measurements per midgut and the error bars are the S.E.M of those averages. Scale bars 1µm.

FIG. 2: Gliotactin is located at the Tricellular junction (TCJ) in differentiated cells in the intestine. (A) Confocal image of posterior midgut showing the localization of Gli-GFP (green) at the TCJ. Scale bar 10µm; n=11. (B-B') Protein localization along the apical-basal axis; note co-localization of Gli-GFP (green) with Dlg (red). Scale bar, 5µm. (C) Gli (green) is localized at TCJ of EC (arrows) and in EE (arrowhead, marked by Prospero in red). Arm (red) localizes to the adherens junction (AJ) in all cells. Scale bar 5µm; n=10 (D) Gli does not co-localize with Dlg, which appears cytoplasmic, in ISC/EB nests (dashed line). Scale bar, 5µm; n=10. (E) EM of an ISC/EB nest. SJs are apparent between ECs (black box), but not between ISC/EBs (red box). Blue box= ISC/EB-EC

contacts. n=11 midguts (n=5 ISC/EB nests were observed per midgut), Scale bar, 1µm. (F-G') Gli is mis-localized from TCJ in posterior midguts from 50do flies; Scale bar, 5µm. Samples dissected and stained in parallel under same conditions, pictures taken at same laser intensity; (F) n=27 midguts, (G) n=22. (H) Fluorescence intensity ratio of Gli at TCJ/Cytoplasm in ECs from young and old flies. Asterisks represent statistically significant difference using an unpaired Student's t-test, two-tailed (**** = P < 0.0001). Error bars are SEM range of those averages. (I) Lifespan curves for female flies raised on conventional food (red)(n=294) or DR food (yellow)(n=223). T50 and total lifespan were significantly lower in controls compared with DR. Data analyzed with non parametric Log-Rank (Mantel-Cox) test; **** = P<0.0001, represent statistically significant difference. (J) TCJ/Cytoplasm fluorescence ratio for Gli shows a slower decrease in DR flies (red) than in control (yellow). Data analyzed with unpaired Student's t test, two tailed, and error bars are the SEM range of those averages. ****= P<0,0001. Each data point (n=midguts) represents an average fluorescence intensity ratio from 2-7 independent measurements per midgut and bars are SEM range of those averages. 10do Ctrl n=20 midguts; 10do DR n=18; 20do Ctrl n=35; 20do DR n=29; 30do Ctrl n=22; 30do DR n=22; 40do Ctrl n=15; 40do DR n=23.

FIG. 3: Loss of Gliotactin in ECs leads to loss of intestinal barrier integrity.

(A) Flies with reduced *Gli* expression (*5966^{GS} GAL4/UAS-Gli^{RNAi}*, RU+, n=265) show acceleration of loss of barrier integrity, when compared to controls (*5966^{GS} GAL4/UAS Gli^{RNAi}* EtOH fed, RU-, n=240 flies). Asterisks represent a statistically significant difference in pairwise post-test comparisons, indicated by the corresponding bars (**** P < 0.0001; ** P < 0.001 and * P < 0.05; Fisher's exact test; two tailed). (B-I) Confocal images of posterior midguts from 23do flies. Loss of Gli in ECs did not affect the levels of SJ proteins Dlg (C; n=18), Cora (E; n=18), Mesh (G; n=18) or Ssk (I; n=18), although disruption of the TCJ and mis-localization of SJ proteins was observed, compared to respective controls (TCJ marked by arrowheads in B, n=16; D, n=16; F, n=19; H, n=16). Samples were dissected and stained in parallel under the same conditions, pictures taken at same laser intensity. (J-M) Depletion of *dlg* induced in ECs with *Myo1A-GAL4 GAL80^{ts} UAS-dlg^{RNAi}* for 7 days. At 29ºC Dlg is reduced from ECs but maintained in EEs (L), while Gli is completely lost from TCJ (M) compared to controls maintained at 18ºC (J-K). Scale bars 10 µm. J-K n=19; L-M n=20.

FIG. 4: Loss of Gliotactin in ECs induces ISC proliferation and accumulation of *esg+* cells. (A-F) Posterior midguts from *Su(H)LacZ; 5966^{GS}GAL4*, *esg:GFP/ UAS-Gli^{RNAi}* flies after 2d (A-B) or 9d (C-D). *Gli* knockdown causes an increase in *esg+* ISC/EBs (marked by esg:GFP, green) and ISC proliferation (marked by arrowheads PH3, red) after 9days (D), comparing to RU- controls (C). (A) n=64 images (4 images taken per midgut n=16 midguts); (B) n=76 (4 images taken per midgut n=19); (C) n=72 (4 images were taken per midgut n=18); (D) n=60 (4 images taken per midgut n=15). (E-F) Graphical summary showing changes in ISC/EB number (E) and mitosis counts (F) after 5 days. (E) Each data point is an average proportion calculated from 4 independent images per midgut and bars are the mean +/- S.E.M of those averages (ONE-way ANOVA/Tukey's multiple comparisons test) ** = P< 0.01, represents a statistically significant difference. (F) Each data point is an average proportion calculated from 4 independent images per midgut and bars are the median with interquartile range of those averages (Kruskal-Wallis/Dunn multiple comparisons test). ** = P< 0.01, represents a statistically significant difference. (G-J). Posterior midguts from *Su(H)LacZ; 5966^{GS}GAL4*, *esg:GFP/ UAS-Gli^{RNAi}* flies raised under axenic conditions. After 7 days of *Gli* depletion, effects on *esg+* cell number and ISC mitoses were still observed. (G-H) *Gli* knockdown caused an increase in the ISC/EBs cell number (marked by esg:GFP, green) and proliferation (marked by arrowheads PH3, red) after 7days (H), comparing to RU- controls (G). (G) n=80 (4 images taken per midgut n=20); (H) n=80 (4 images taken per midgut n=20) (I-J) Graphical summary showing the statistical significance in ISC/EB number (I) and mitosis counts (J) after 7 days. (I) Each data point is an average proportion calculated from 4 independent images per midgut and the bars are the mean +/- S.E.M of those averages (unpaired Studen's t-test, two tailed) **** = P< 0.0001, represents a statistically significant difference. (J) Each data point is an average proportion calculated from 4 independent images per midgut and bars are the median with interquartile range of those averages (Mann-Whitney non-parametric test). ** = P< 0.01, represents a statistically significant difference. Scale bars 10μm.

FIG. 5: JNK signaling is activated downstream of Gli to drive changes in ISC behavior in a non-autonomous manner. (A-F') Reduction of *Gli* expression in ECs using *5966 GAL4^{GS}* triggers JNK pathway activation, reported by *puc-lacZ* expression (red or grey) in ECs 2 (B-B'; n=11 midguts), 5 (D-D'; n=8) and 9 (F-F'; n=8) days after reducing *Gli* expression, compared to RU- controls (A-A', n=7; C-C', n=8; E-E', n=7).

ISC/EB marked by esg-GFP (green), cell nuclei by DAPI (blue). (G-Q) Epistasis analysis between Gli (Gli^{RNAi}) and Bsk (BSK^{DN}). Midguts were stained with DAPI (nuclei, blue), GFP (*esg+* cells, green) and PH3 (mitotic cells, red) following 9 days of incubation in RU+ or RU. We observe that blocking JNK signaling (Bsk^{DN}) (*5966^{GS} GAL4/UAS-Gli^{RNAi} UAS-Bsk^{DN}*, RU+) (N;O-P) rescues the non-autonomous effect on ISC proliferation produced by Gli^{RNAi} (*5966^{GS} GAL4/UAS-Gli^{RNAi}*, RU+)(J, O-P). (O) ISC/EB counts in midguts. Each data point is an average proportion calculated from 4 independent images per midgut and bars are the mean +/- S.E.M of those averages (ONE-way ANOVA/Tukey's multiple comparisons test). (P) Quantification of mitotic ISCs. Each data point is an average proportion calculated from 4 independent images per midgut and bars are the median with interquartile range of those averages (Kruskal-Wallis/Dunn multiple comparisons test) **** = P< 0.0001, represent statistically significant difference. (Q) Quantification of loss of barrier function. Flies with reduced *Gli* expression (*5966^{GS} GAL4/UAS-Gli^{RNAi}*, RU+, n=259) present the same increase on Smurf proportion than the combination Gli^{RNAi} Bsk^{DN} (*5966^{GS} GAL4/UAS-Gli^{RNAi} UAS-Bsk^{DN}*, RU+, n=264), compared to Bsk^{DN} (*5966^{GS} GAL4/UAS-Bsk^{DN}*, RU+, n= 277) and controls flies (*5966^{GS} GAL4/UAS-Gli^{RNAi}* EtOH, RU-, n=290). Fisher's exact test; two tailed. **** = P<0.0001, *** = P<0.001, ** = P< 0.01, * = P<0.05 represent statistically significant difference. Scale bars, 10 μm. (M) n=80 (4 images taken per midgut n=20); (H) n=80 (4 images taken per midgut n=20); (I) n=76 (4 images taken per midgut n=19); (J) n=80 (4 images taken per midgut n=20); (K) n=72 (4 images taken per midgut n=18); (L) n=64 (4 images taken per midgut n=16); (M) n=88 (4 images taken per midgut n=22); (N) n=96 (4 images taken per midgut n=24).

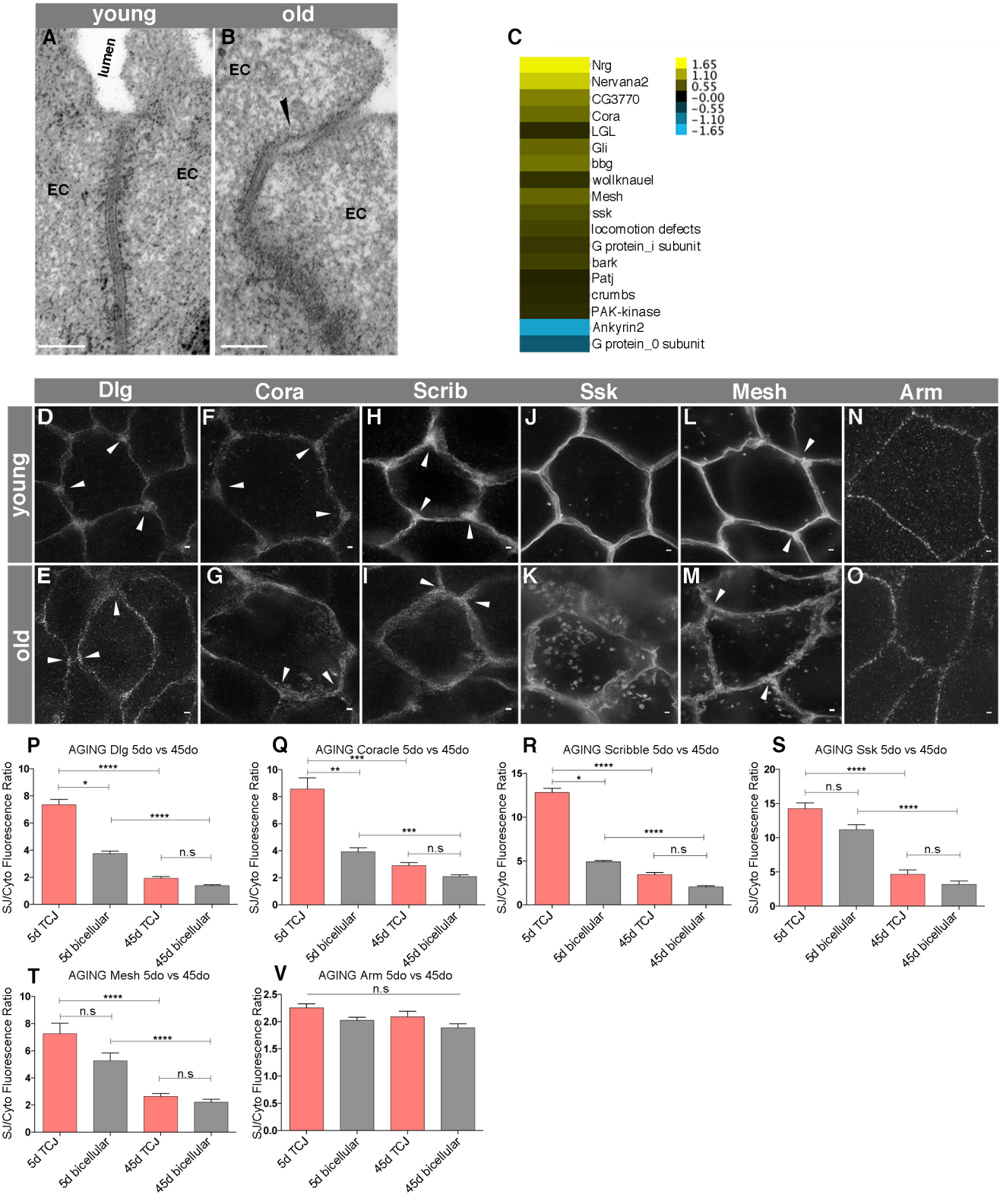

Resnik-Docampo *et al.* Fig. 1

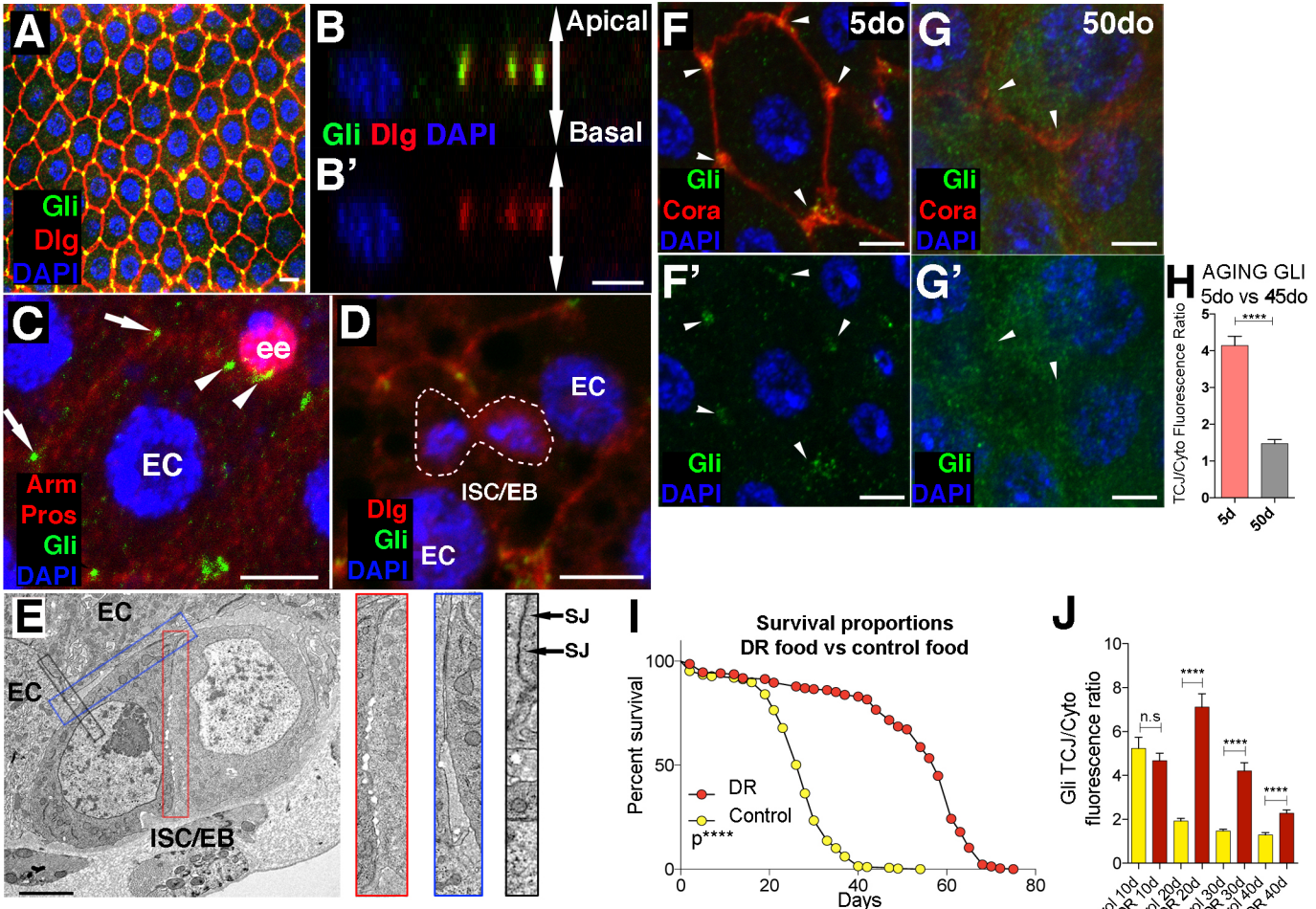

Resnik-Docampo *et al.* Fig. 2

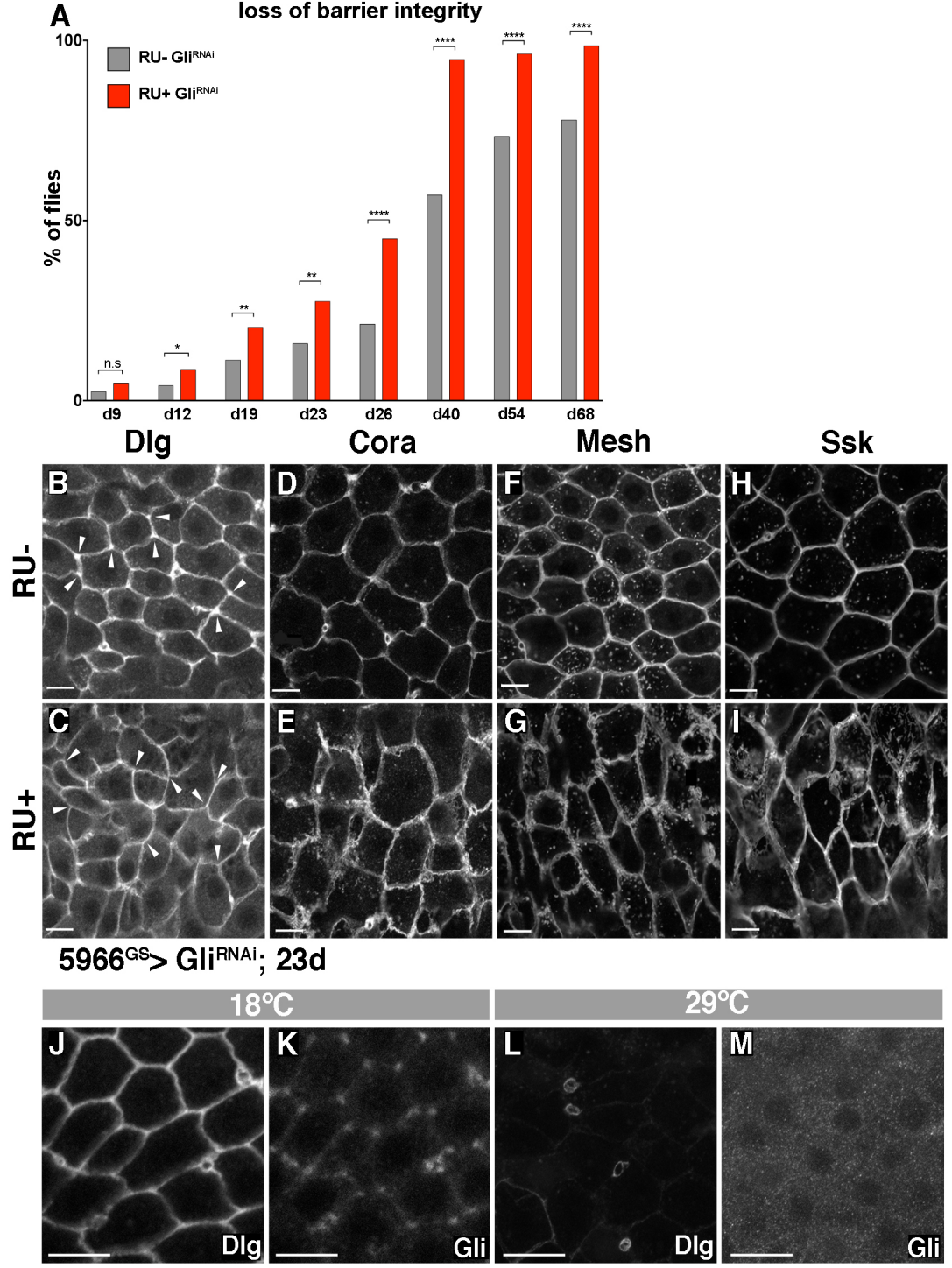

Resnik-Docampo *et al.* Fig. 3

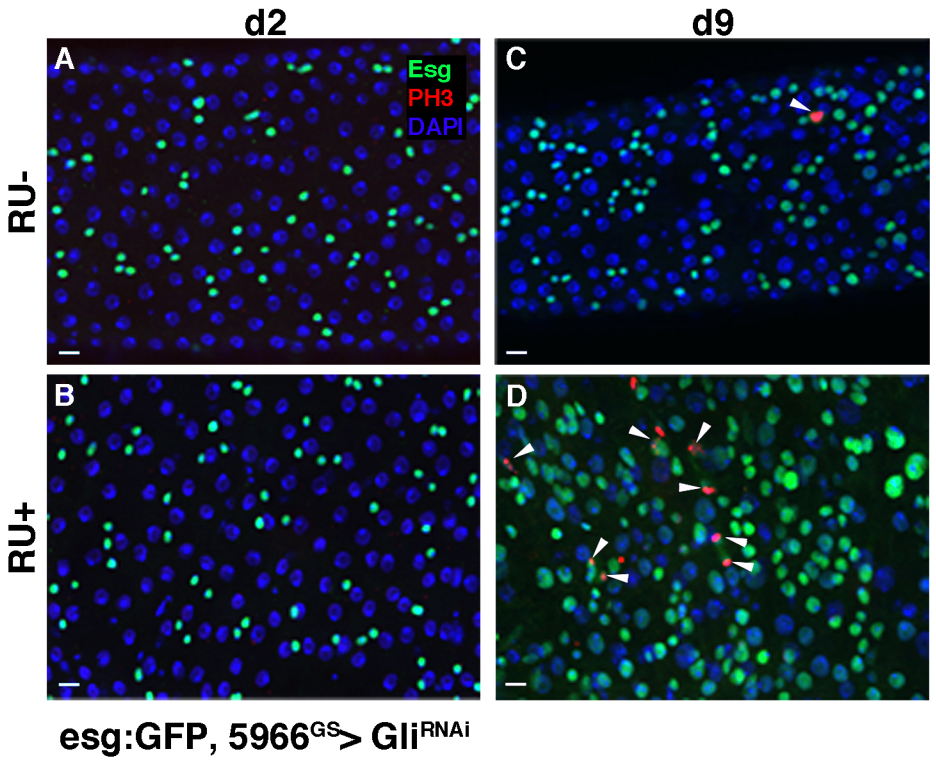

esg:GFP, 5966^{GS}> Gli^{RNAi}

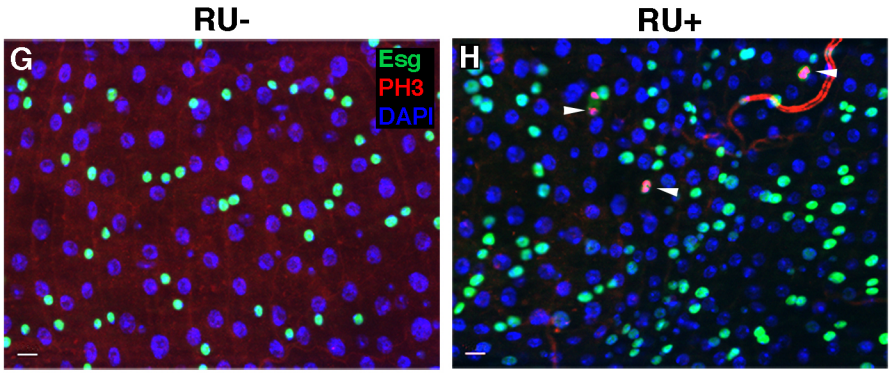

esg:GFP, 5966^{GS}> Gli^{RNAi}, 7d, axenic

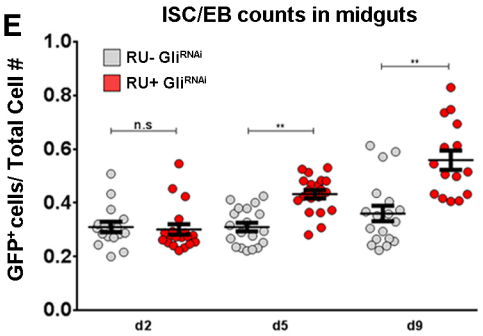

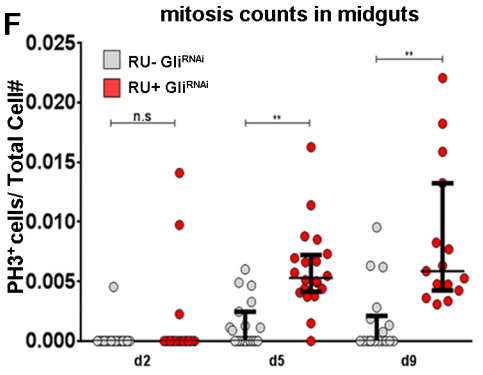

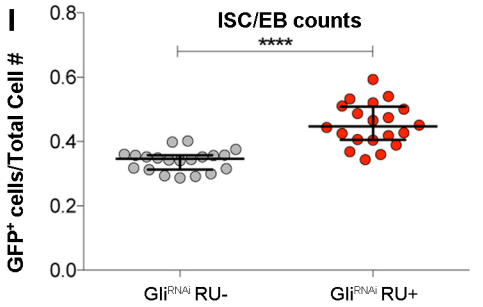

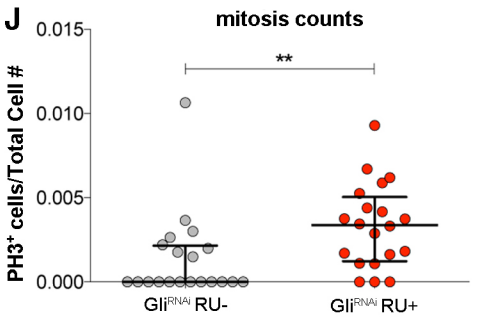

Resnik-Docampo *et al.* Fig. 4

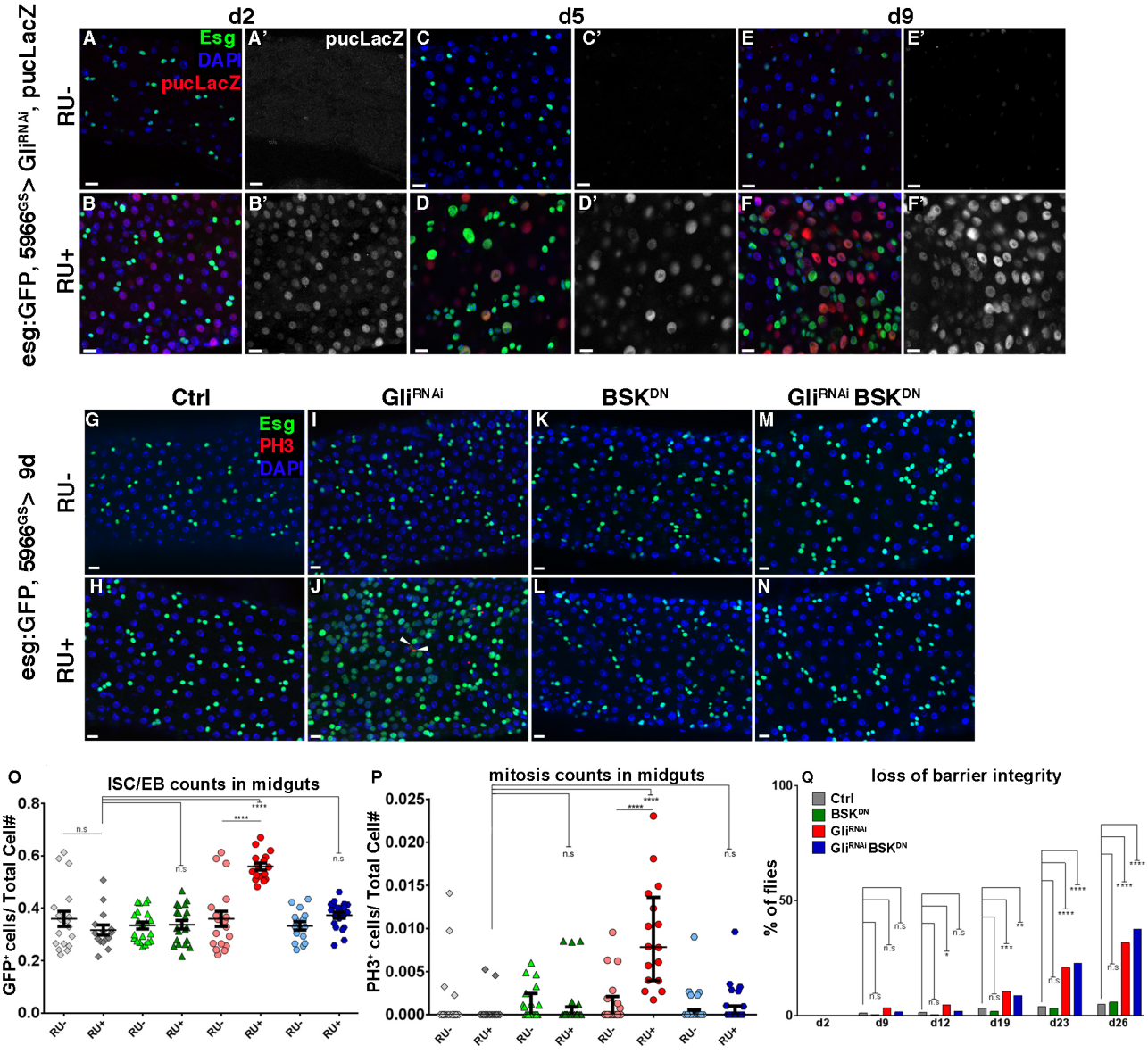

Resnik-Docampo *et al.* Fig. 5

Materials & Methods

Fly food and husbandry

Flies were cultured in vials containing standard cornmeal medium (1% agar, 3% brewer's yeast, 1.9% sucrose, 3.8% dextrose, and 9.1% cornmeal; all concentrations given in wt/vol). Dietary restriction diet[9]: 1% agar, 0.55% brewer's yeast, 5% sucrose, and 8.6 % cornmeal; all concentrations given in wt/vol. Control food for DR diet: 1% agar, 5.5% brewer's yeast, 5% sucrose, and 8.6 % cornmeal; all concentrations given in wt/vol. Two inducible GAL4/UAS systems were used in this study: the GeneSwitch system [19, 20], and the Target system[32]. All crosses with the GeneSwitch driver were carried out at 25°C. Crosses with the TARGET system were set up and maintained at 18°C until eclosion. In both cases, adults were kept for an additional 2-3 days, and induced at 3-4 days after eclosion by placement on food containing the steroid hormone mifepristone (RU486; Sigma M8046) in a 25µg/mL concentration, and flipped every 2 days thereafter. All analyses for these studies were performed on female flies, as age-related gut pathology has been well established in females[6, 9].

Fly Stocks used

Unless otherwise stated, crosses were done at 25ºC. Lines not described in the text can be found in Flybase. *UAS-Bsk^{DN}*, *UAS-dIAP, UAS-P35* and *puc-lacZ* [33]. Gal4 lines: *Su(H)lacZ; esg:GFP,5966GAL4^{GS}* (gift from B. Ohlstein); *Myo1AGAL4,* UAS-*GAL80^{TS}* ; *Sal^{EP}GAL4* ([34], gift from JF. de Celis); *Rab3GAL4*, *tubGAL80$^{TS.}$*. Lines used for RNAi-mediated knock-down: *UAS-Gli^{RNAi}* (37115GD,VDRC); *UAS-Gli^{RNAi}* (37116GD,VDRC); *UAS-Gli^{RNAi}* (107258KK, DSRC); *UAS-Ssk^{RNAi}* (11906GD,VDRC); *UAS-mesh^{RNAi}* (11906GD,VDRC); *UAS-bbg^{RNAi}* (15975GD,VDRC); *UAS-cora^{RNAi}* (9787GD,VDRC); *UAS-scrib^{RNAi}* (29552, BDCS); *UAS-dlg^{RNAi}* (25780, BDSC). GFP protein trap lines: Gli:GFP (115-332, DGRC); Scribble:GFP, Neuroglian:GFP, NeurexinIV:GFP, Nervana:GFP (gifts from G. Tanentzapf).

Transmission Electron Microscopy

Tissues were fixed in 2.5% glutaraldehyde, in 0.1M phosphate buffer, 0.9% sodium chloride (PBS) and washed. The tissues were treated with 1% OsO4 with 0.3 % potassium ferrocyanide in PB for 1 hour, followed by 2% UA for 1 hour. The tissues then were dehydrated in a graded series of ethanol, treated with propylene oxide and embedded in Eponate 12 (Ted Pella). Approximately 50-60 nm thick sections were cut

on a TMC ultramicrotome and picked up on formvar coated copper grids. The sections were stained with uranyl acetate and Reynolds lead citrate and examined on a JEOL 100CX electron microscope at 60kV.

Fluorescence Microscopy and Antibody staining

Our observations were carried out in the P3-P4 regions of the *Drosophila* intestine located by centering the pyloric ring in a 40× field of view (fov) and moving 1–2 fov toward the anterior. Posterior midguts were dissected into ice-cold PBS/4% formaldehyde and incubated for 1hr in fixative at room temperature. Samples were then washed three times, for 10 min each, in PBT (PBS containing 0.5%Triton X-100), 10 min in Na-deoxycholate (0.3%) in PBT (PBS with 0.3%Triton X-100), and incubated in block (PBT-0.5% bovine serum albumin) for 30 min. Samples were immunostained with primary antibodies overnight at 4°C, washed 4 × 5 min at RT in PBT, incubated with secondary antibodies at RT for 2 h, washed three times with PBT and mounted in Vecta-Shield/DAPI (Vector Laboratories, H-1200).

The following antibodies were obtained from the Developmental Studies Hybridoma Bank, developed under the auspices of the NICHD and maintained by The University of Iowa, Department of Biology, Iowa City, IA 52242. Discs large (mouse, 1:20, 4F3) and Coracle (mouse, 1:20, C615.16). GFP (rabbit, 1:3,000, Molecular Probes A-11122); GFP (mouse, 1:200, Molecular Probes A-11120); GFP (chicken, 1:500, Aves Labs GFP-1010); β-GAL (rabbit, 1:2000, Cappel/ MPbio 559761); Phospho-histone3 (rabbit, 1:200, Millipore 06-570). Gliotactin (mouse, 1:50, gift from V. Auld); Snakeskin (rabbit, 1:1000) and Mesh (rabbit, 1:1000) (gifts from M. Furuse).

Images were acquired on a Zeiss LSM710 inverted confocal microscope, and on a Zeiss Axio Observer Z1 and processed with Fiji/ImageJ and Zen from Zeiss. Super resolution images were obtained from a custom build Stimulated Emission Depletion (STED) super resolution microscope currently reaching a resolution of about 30-40nm[35]. The STED system was built in the Dept of Anesthesiology, UCLA. Supported an NIH grant from the National Heart, Lung, and Blood Institute BRG R01 HL088640. Final figures were assembled using Adobe Photoshop.

TCJ and Bicellular septate junction fluorescence quantification

To measure and compare the TCJ or Bicellular SJ fluorescence intensity of Gli-GFP, Dlg, Cora, Sribble-GFP, Mesh and Ssk in posterior midguts ECs, 100x + 3X of digital magnification confocal z-stack maximum projections at the level of the TCJ and SJ were generated using Zen 2 pro Blue software edition (Zeiss). TCJ were manually localized using Gli-GFP and a SJ marker (Ssk, Cora, Dlg or Mesh). TCJ and SJ fluorescence intensity were measured using a mask of 25.5 pixels diameter. Then cytoplasm fluorescence intensity were calculated using the same mask. Average fluorescence intensity at TCJ or SJ was divided by the cytoplasmic average intensity. Between 3 to 7 measurements were taken per picture and a minimum of 20 posterior midguts were analyzed per experimental condition.

Quantification using CellProfiler

For statistical significance four images were taken as z-stacks with a typical slice thickness of 750 nm. per posterior midgut; two on each side (top and bottom); from contiguous field of view, starting at 1 fov from the pylorus (using a minimum of 20 guts). The images were then processed using CellProfiler [36] pipeline developed in the Jones lab. ISC number and mitotic events were obtained from esg:GFP/total cell and PH3/total cell ratios respectively. Average ratios from the four images corresponding to a single gut were used in subsequent statistical analyses.

Statistics and reproducibility

Statistical analysis and graphical display of the data were performed using Prism6 (GraphPad). Significance, expressed as p values, was determined with a two-tailed test, the following parametric or non-parametric tests were used as indicated in figure legends: ANOVA/Tukey's multiple comparisons test or Student's t-test were used when data met criteria for parametric analysis (normal distribution, equal variances), Kruskal-Wallis/Dunn multiple comparisons test was used when data were non-parametric, Fisher's exact test, Log-rank (Mantel-Cox) test. Experiments were repeated at least two times.

Barrier integrity assays ('Smurf' assay)

Flies were maintained on standard medium prepared with FD&C Blue Dye nº1 from Spectrum added at a concentration of 2.5% (wt/vol). Loss of intestinal barrier function

was determined when dye was observed outside of the digestive tract as described in [8, 9].

Generation of axenic flies

Embryos were treated as described previously [26, 37]. Eight to fourteen hour old embryos were collected on grape agar plates using commercially available cages (flystuff.com). Embryos were dechorionated in 3% sodium hypochlorite (50% v/v regular bleach) for 20 min, rinsed in 70% ethanol for 5 min, and then washed three times with in PBS + 0.01% Triton X-100. Axenic embryos were transferred to autoclaved medium (50 embryos/vial) in a laminar flow cabinet. Axenic conditions were confirmed via plating fly homogenate, as well as by plating of swabs from spent vials, on de Man, Rogosa, Sharpe (MRS) bacterial agar, prior to each time point. Microbe-associated controls were generated by adding 60 uL whole fly homogenate (1 fly equivalent, from a glycerol stock of conventionally reared flies) per vial to embryos post sterilization, as described previously[26].

RNA extraction

Seventy-five female posterior midguts or 5 whole flies per condition after dissection were frozen at -80ºC in fresh trizol buffer (TRizol Reagent, Life Technologies, 15596026; 5µg Linear Poly-Acrylamide Sigma 56575, 100ηg of tRNA). Total RNA was extracted pooling midgut samples, followed by 5 rounds of freezing (liquid nitrogen)/thawing at 37ºC in a water bath. Samples then underwent 5 rounds of vortexing at RT for 30'', letting stand at RT for 5 min to disrupt all RNA-protein complexes. Finally RNA was isolated by phenol/chloroform extraction. Purified RNA was treated with DNase Q1 (Promega, M610A).

Quantitative RT-PCR and PCR

RNA (2µg) from posterior midguts dissected from RU486 (RU+) or EtOH (RU-) fed flies (genotypes: *Su(H)lacZ; esgGFP, 5966GAL4*^{GS} crossed to UAS-*Gli*^{RNAi}) was reverse-transcribed using the iScriptkit (Bio-Rad, 170-8841). Standard qPCRs were carried out on a Bio-Rad CFX96/C1000 Touch system (Bio-Rad), using Sso Advanced SYBR Green (Bio-Rad, 1725-264). The following primer sequences were used: RpL32 Fwd: ATCGTGAAGAAGCGCACCAA; RpL32Rev: TGTCGATACCCTTGGGCTTG; Gli Fwd: GCCGAATCGTCCAATTACAG; Gli Rev: ACTTTAAAGAAAAATTCCAGGAGAAA; Puc

Fwd: CGACTTTATCGAAGATGCACGG; PUC Rev: CAGGGAGAGCGACTTGTACC. Expression levels of targets analyzed were calculated relative to RpL32 expression, using the ΔΔCt method.

Transcriptome analysis (RNA sequencing)

RNA-Seq libraries were prepared from three biological replicates for each experimental condition. The NEBNext poly(A)-mRNA magnetic isolation kit (NEB E7490S) was used to isolate poly(A)-mRNA from 4 µg of whole mRNA. cDNA libraries were generated using the NEBNext RNA Library Prep Kit for Illumina (NEB E6110S), and NEBNext Multiplex Oligos for Illumina (NEB E7335S) were used for multiplexing. All steps were performed according to manufacturer's directions. RNA sequencing was performed on a Hi-Seq2000 (Illumina) with 50 bp single-end read length.

Bioinformatics analysis

Genomatix software from was used for mapping spliced reads, making transcript assemblies, and for differential expression analysis. Reads were first trimmed by removing adapter and Illumina-specific sequences. Next, trimmed reads were aligned against the *Drosophila* genome (NCBI el dorado version 08.2011) with default settings. Finally, a differential expression analysis was performed using the DESeq package method with a P-value threshold of $p<0.05$. Differentially expressed genes were interrogated for overrepresented biological themes using database for annotation visualization and integrated discovery (DAVID) and categorized based on GO terms. The DAVID functional annotation clustering tool highlights the most relevant GO terms associated with a differentially expressed gene list. Details of the DAVID algorithm can be found at http://david.abcc.ncifcrf.gov/.

Data availability

The RNAseq data discussed in this publication have been deposited in NCBI's Gene Expression Omnibus and are accessible through GEO Series accession number GSE74168, GSE74171, GSE74172.

https://www.ncbi.nlm.nih.gov/geo/query/acc.cgi?acc=GSE74168
https://www.ncbi.nlm.nih.gov/geo/query/acc.cgi?acc=GSE74171
https://www.ncbi.nlm.nih.gov/geo/query/acc.cgi?acc=GSE74172

Source data for Fig. 1C have been provided as a Supplementary table 1. All other data supporting the findings of this study are available from the corresponding author on request.

References for Materials and Methods:

32. McGuire, S.E., Mao, Z. & Davis, R.L. Spatiotemporal gene expression targeting with the TARGET and gene-switch systems in Drosophila. *Science's STKE : signal transduction knowledge environment* 2004, pl6 (2004).
33. Martin-Blanco, E. *et al.* puckered encodes a phosphatase that mediates a feedback loop regulating JNK activity during dorsal closure in Drosophila. *Genes & development* 12, 557-570 (1998).
34. Cruz, C., Glavic, A., Casado, M. & de Celis, J.F. A gain-of-function screen identifying genes required for growth and pattern formation of the Drosophila melanogaster wing. *Genetics* 183, 1005-1026 (2009).
35. Mitchell-Jordan, S. *et al.* Features of endogenous cardiomyocyte chromatin revealed by super-resolution STED microscopy. *Journal of molecular and cellular cardiology* 53, 552-558 (2012).
36. Carpenter, A.E. *et al.* CellProfiler: image analysis software for identifying and quantifying cell phenotypes. *Genome biology* 7, R100 (2006).
37. Bakula, M. The persistence of a microbial flora during postembryogenesis of Drosophila melanogaster. *Journal of invertebrate pathology* 14, 365-374 (1969).

Extended Data:

Supplementary Fig. 1: Localization of septate junction (SJ) proteins in the intestinal tract in young and aged flies.. Related to Fig1 and Fig2F-G

Supplementary Fig.2: Verification of Gli reagents. Data related to Figs. 3-5.

Supplementary Fig. 3: Effects of Gli depletion in the posterior midgut. Extended data related to Fig.4

Supplementary Fig. 4: Neither changes in bacteria nor death of ECs induces changes in ISC behavior downstream of Gli. Extended data related to Fig. 5

Supplementary Table 1: RNAseq data of gene expression changes in posterior midguts from young and old flies

Supplementary Table 2: RNAseq data of gene expression changes in posterior midguts from flies in which *Gliotactin* is reduced specifically in enterocytes for 2 or 9 days

Figure Legends

FIG. 1: Localization of septate junction (SJ) proteins in the intestinal tract in young and aged flies. (A) Schematic representation of a *Drosophila melanogaster* midgut (B-I) Localization of SJ proteins in posterior midgut and hindgut of young flies. (B; n=4 midguts) Nervana:GFP, (C; n=5) Neurexin IV:GFP, (D; n=11) Neuroglian:GFP, (E; n=7) Snakeskin, (F; n=6) Scribble:GFP, (G; n=10) Discs large, (H; n=6) Coracle, (I; n=6) Mesh. Scale bars, 0.1mm. (J-S) No changes in SJ protein levels were observed in hindguts from aged flies. STED (J-O) and confocal (P-Q) images comparing SJ proteins localization of 10do hindguts to 45do, scale bars 1µm and 5µm. (R-S) STED images showed the AJ protein Arm localization is not affected by aging, scale bars 1µm. n=>14 hindguts per condition (n=10 ECs were observed per hindgut). Samples were dissected and stained in parallel under same conditions, pictures taken at same laser intensity.

FIG. 2: Verification of Gli reagents. (A-C) GLI:GFP and anti-GLI co-localization (wing discs). GliRNAi efficiency demonstrated by immunofluorescence (IF) microscopy (wing discs) and qPCR (posterior midguts). (A-A'') Wing disc peripodial membrane showing the co-localization of Gli-GFP (green) with Gli (red), DAPI (blue); Scale bars, 10µm; n=16. (B-C) Gli protein is localized at the TCJ between wing cells (red signal in B; n=14) in wild type discs. Gli is strongly reduced in discs expressing GliRNAi (*SalPE-GAL4 UAS-GFP UAS-Gli^{RNAi}*, C; n=12). Scale bars, 50µm. (D) RT-qPCR of posterior midguts *5966^{GS} GAL4/UAS-Gli^{RNAi}* flies RU+ and RU- showing a decrease of *Gli* expression after 5 and 9 days post Gli^{RNAi} expression. n=75 females posterior midguts per condition. Bars are the mean +/- S.E.M (two tailed, unpaired Student's t-test). *** = P<0.001, ** = P<0.01 represent a statistically significant difference. (E) Flies fed with EtOH (light blue) (*5966^{GS} GAL4/+*, RU-, n=270) show no statistical difference in number of flies that have lost barrier function, when compared to those fed RU (blue) (*5966^{GS} GAL4/+* fed, RU+, n=268). Fisher's exact test; two tailed. (F-G) EM images of SJ (arrowheads) between adjacent ECs in guts from 23do *5966^{GS} GAL4/UAS-Gli^{RNAi}* flies (RU+, n=12) (G) compared to control flies (F) *5966^{GS} GAL4/UAS-Gli^{RNAi}* (RU-, n=15). For each midgut n=9 EC/EC Septate Junctions were observed per experimental condition. Scale bars, 0.1µm (H) Lifespan curves of *5966^{GS} GAL4/UAS-Gli^{RNAi}* [(RU+, red)(n=265) and RU- (grey)(n=240)] female flies. T50 was significantly lower in RU+ d30 compared with RU-

d37. Data analyzed with non parametric Log-Rank (Mantel-Cox) test; *** = P<0.001, represent a statistically significant difference.

FIG. 3: Effects of Gli depletion in the posterior midgut. (A-F) *5966^{GS} GAL4; esg-GFP* flies (RU+ or RU-) crossed with RNAi lines targeting Gli or Dlg. (A-D) Multiple *Gli*^{RNAi} lines induce an increase of ISC/EB cells, when expressed (RU+) (B, n=12; D, n=11) compared to RU- controls (A, n=11; C, n=9), similar to results presented in Fig.4D. (E-F) Depletion of Dlg (*dlg*^{RNAi}, RU+) (E, n=15) induces an increase in ISC/EBs compared to controls (RU-) (F, n=14). (G-K) Changes in ISC/EB number after *Gli* depletion are reversible (*5966^{GS} GAL4; esg-GFP UAS-Gli^{RNAi}* RU+, RU-) (G) Graphical summary showing the statistical significance in changes in ISC/EB number depicted in H-K. (H) Intestine from *5966^{GS} GAL4; esg-GFP UAS-Gli^{RNAi}* (fed RU+) for 9 days. (I) Flies were shifted onto food containing EtOH (RU-) to re-initiate Gli expression for 11 days. Re-expression of Gli resulted in resumption of normal ISC behavior and morphology compared to guts from 20do RU- *5966^{GS} GAL4; esg-GFP UAS-Gli^{RNAi}* controls (J) or guts from 20do *5966^{GS} GAL4; esg-GFP Gli^{RNAi}* flies fed RU+ (K). Scale bars 10μm. Each data point is an average proportion calculated from 4 independent images per midgut and bars are the mean +/- S.E.M of those averages (ONE-way ANOVA/Tukey's multiple comparisons test). **** = P< 0.0001, *** = P<0.001, ** = P<0.01 represent a statistically significant difference. (H) n=60 (4 images taken per midgut n=15); (I) n=76 (4 images taken per midgut n=19); (J) n=84 (4 images taken per midgut n=21); (K) n=80 (4 images taken per midgut n=20) (L) Graphical summary showing that depletion of Gli from EEs using *Rab3-GAL4, tubGAL80^{TS}* for 6d at 29ºC (red) did not result in any changes in ISC behavior, compared to control flies (y,w^{1118}; grey). Each data point is an average proportion calculated from 4 independent images per midgut and bars are the median with interquartile range of those averages (Kruskal-Wallis/Dunn multiple comparisons test). (M-N) No significant differences were detected in AMP expression, after 2, 5, 9 and 21 days post GliRNAi expression. ** = P<0.01, represent statistically significant difference. (M) Drosomycin, (N) Diptericin. n=6 replicates of 5. Boxplots display the first and third quartile, with horizontal bar at the median and whiskers showing the most extreme data point, which is no more than 1.5 times the interquartile range from the box.

FIG 4: Neither changes in bacteria nor death of ECs induces changes in ISC behavior downstream of Gli. (A-F) Epistatic analysis between Gli and apoptosis inhibitors. (A)

ISC/EB counts in flies of indicated genotupes. Each data point is an average proportion calculated from 4 independent images per midgut and bars are the mean +/- S.E.M (ONE-way ANOVA/Tukey's multiple comparisons test). (B) Mitosis counts in midguts from flies of indicated genotypes. Each data point is an average proportion calculated from 4 independent images per midgut and bars are the median with interquartile range (Kruskal-Wallis/Dunn multiple comparisons test) **** = P< 0.0001, represent statistically significant difference. (C-F) IF images of midguts from flies of indicated genotypes stained with DAPI (nuclei, blue), GFP (*esg*+ cells, green) and PH3 (mitotic cells, red, arrowheads) following 9 days of incubation in RU+ or RU-. Co-expression of Gli^{RNAi} with dIAP (*5966^{GS} GAL4/UAS-Gli^{RNAi}; UAS-dIAP*, RU+) or P35 (*5966^{GS} GAL4/UAS-GliRNAi; UAS-P35*, RU+ (A-B; E-F) does not rescue the effect on ISCs produced by depletion of Gli (*5966^{GS} GAL4/UAS-Gli^{RNAi} UAS-LacZ*, RU+)(A-B, D). Compare to control flies fed EtOH (RU-) (*5966^{GS} GAL4/UAS-Gli^{RNAi} UAS-LacZ*, RU-)(A-B, C). (C) n=80 (4 images taken per midgut n=33); (D) n=132 (4 images taken per midgut n=33); (E) n=132 (4 images were taken per midgut n=19); (F) n=68 (4 images taken per midgut n=17). (G-H') Under axenic conditions, reduction of *Gli* expression in ECs still initiates JNK pathway activation, as reported by *puc-lacZ* expression (G, H: red or G', H': grey) in ECs 2 days after reducing *Gli* expression (H-H', n=13), compared to RU- controls (G-G', n=11). ISC/EBs marked by esg-GFP (green), cell nuclei marked by DAPI (blue). (I) MRS plates showing absence of bacterial colonies from cultured fly homogenates of axenic flies at 7do. (J) RT-qPCR of posterior midguts from *5966^{GS} GAL4/UAS-Gli^{RNAi}* flies (RU+ and RU-) showing an increase of *puc* expression after 2, 5, 9 days post Gli^{RNAi} expression. n= 75 females posterior midguts per condition. Bars are the mean +/- S.E.M (two tailed, unpaired Student's t-test). *** = P<0.001, ** = P< 0.01, * = P<0.05 represent statistically significant difference. (K) Lifespan curves of *5966^{GS} GAL4* RU+ female flies crossed with *yw^{118}* (grey, n=290), *UAS-Bsk^{DN}* (green, n=277), *UAS-Gli^{RNAi}* flies (red, n=259) and Gli^{RNAi} UAS-Bsk^{DN} (blue, n=264). ●●●P < 0.001, non parametric Log-rank (Mantel-Cox) test. Scale bars, 10 μm

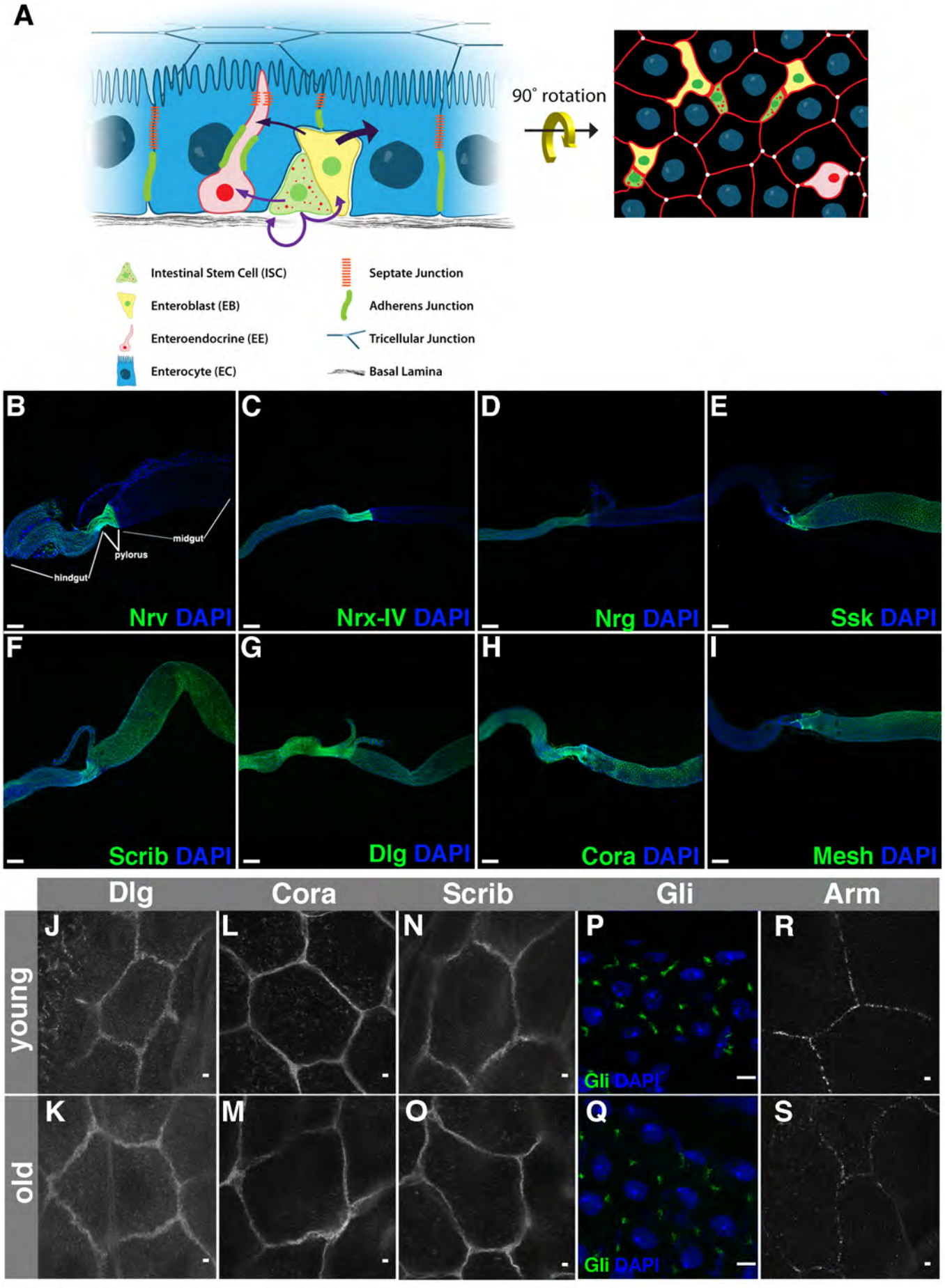

Resnik-Docampo *et al.* Sup. Fig. 1

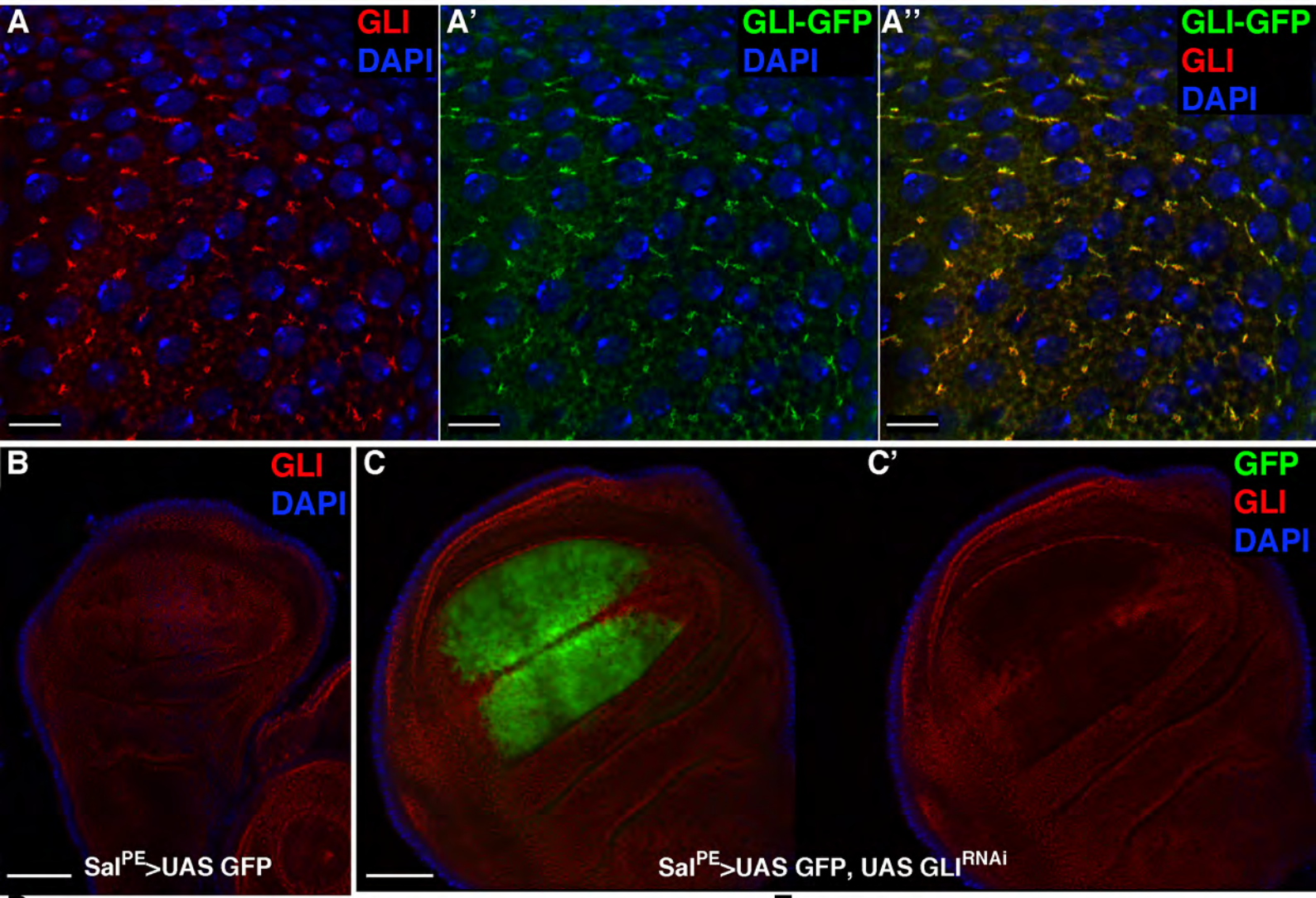

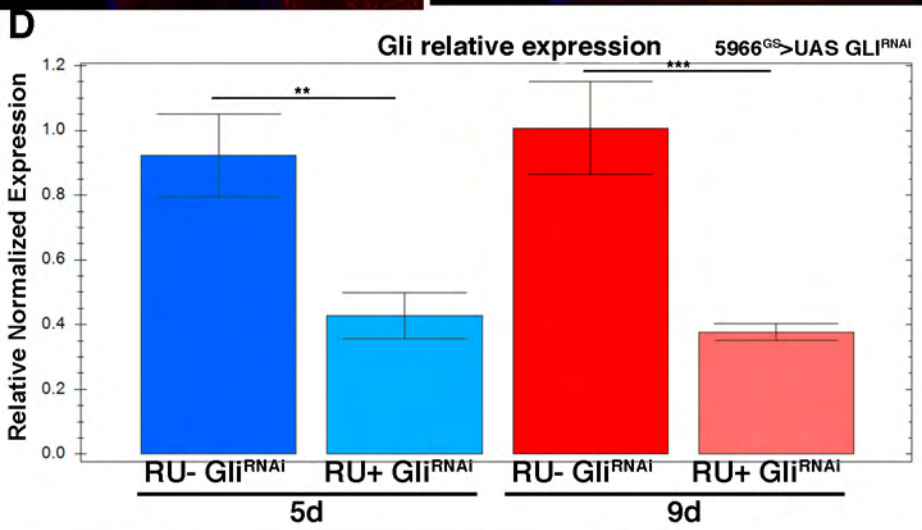

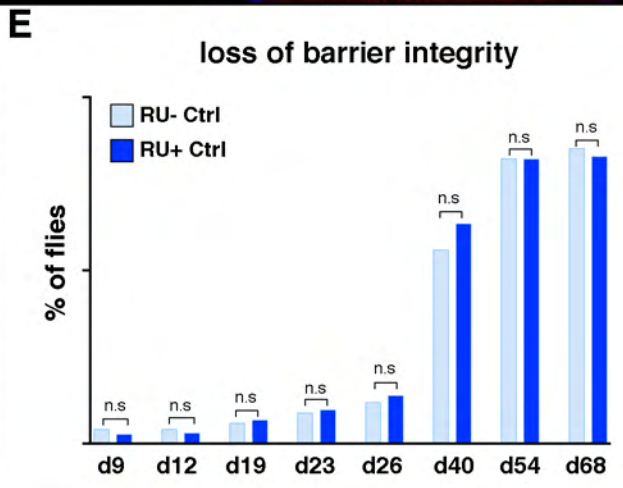

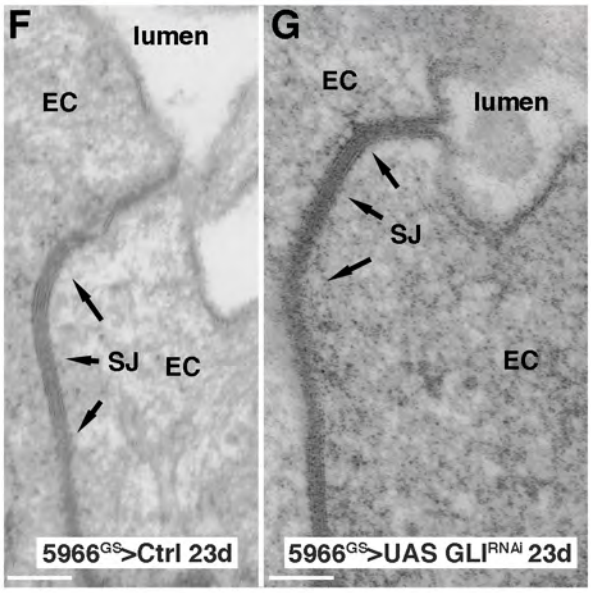

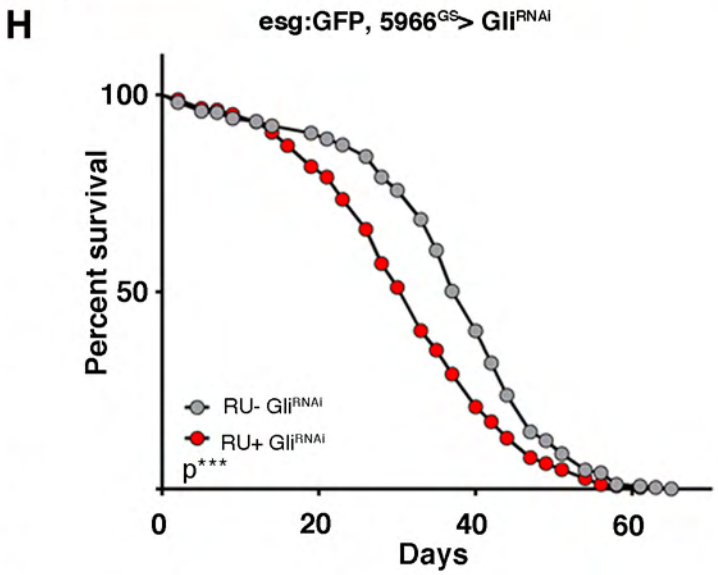

Resnik-Docampo *et al.* Sup. Fig. 2

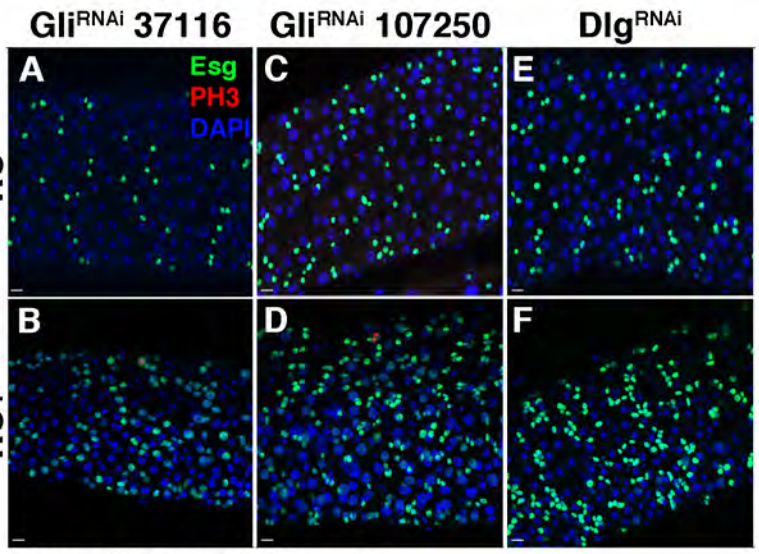

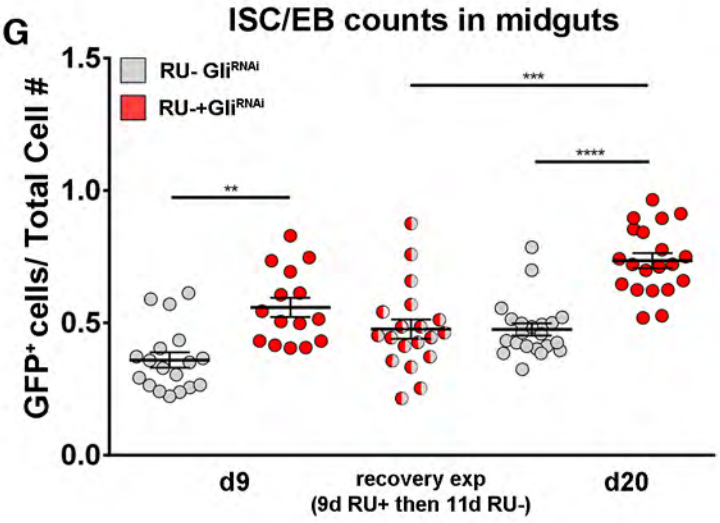

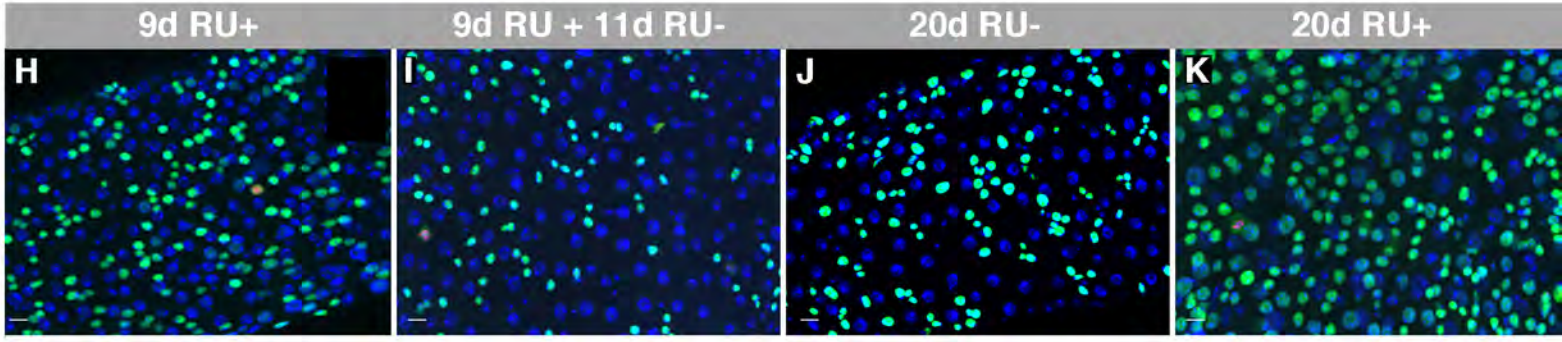

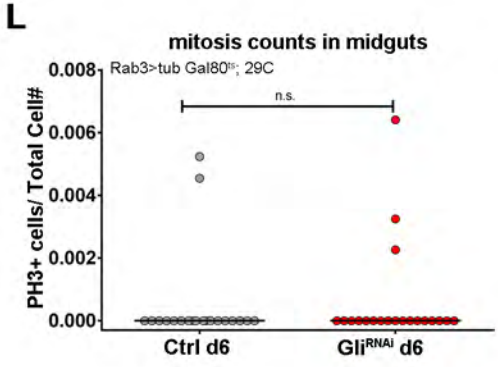

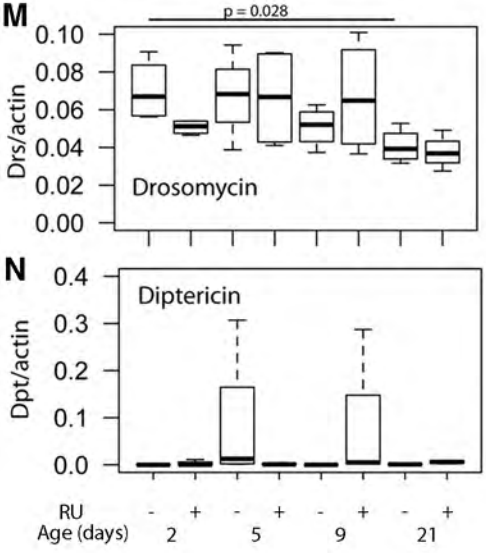

Resnik-Docampo *et al.* Sup. Fig. 3

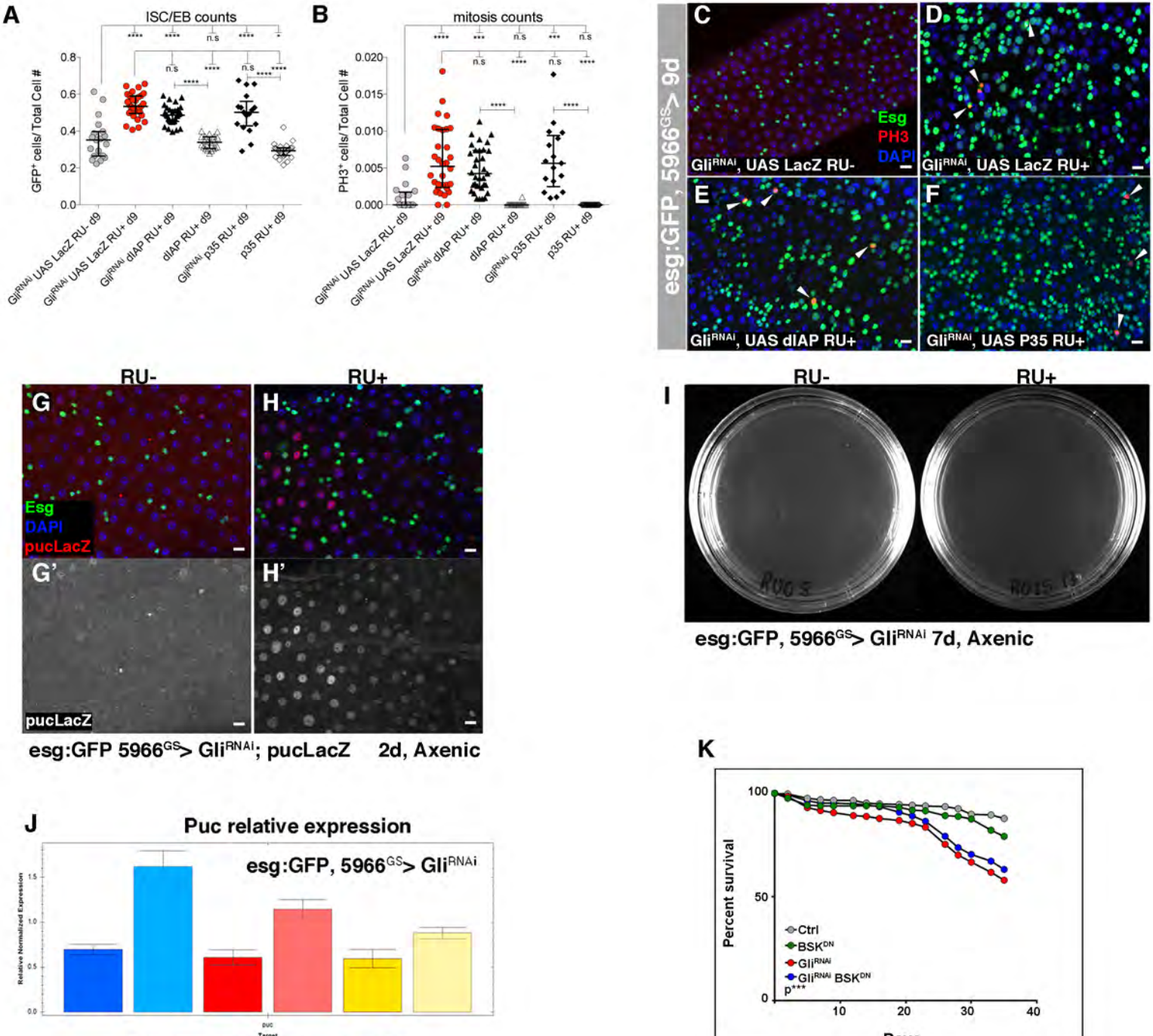

Resnik-Docampo *et al.* Sup. Fig. 4